

SUPERCritical FIELDS, EXTREME NEUTRON-RICH ISOTOPES, AND SHORT LIVING GIANT ATOMS

W. GREINER

*Frankfurt Institute for Advanced Studies, J.W. Goethe-Universität
60438 Frankfurt am Main, Germany
greiner@fias.uni-frankfurt.de*

Received 23 December 2007

Communicated by Guest Editorial Board

The decay of the vacuum in supercritical Coulomb fields is discussed. Connected with that is the time delay in giant nuclear systems like U+Cm etc. This – in turn – is connected with the production of superheavy elements. Recent theoretical and experimental studies of extreme neutron-rich isotopes are also mentioned. A perspective for future research is given.

Keywords: Quantum electrodynamics; strong fields; superheavy nuclei; giant quasi-atoms.

1. The Vacuum in Quantum Electrodynamics

It is generally accepted that the physical vacuum has a nontrivial structure. This conclusion was first made by Dirac on the basis of his famous equation for a fermion field which describes simultaneously particles and antiparticles. The Dirac equation in the vacuum has a simple form

$$(i\gamma^\mu \partial_\mu - m)\Psi(x) = 0, \quad (1)$$

where $\gamma^\mu = (\gamma^0, \boldsymbol{\gamma})$ are Dirac matrices, m is the fermion mass and $\Psi(x)$ is a 4-component spinor field. For a plane wave solution $\Psi(x) = e^{-ipx}u_p$ this equation is written as

$$(\hat{p} - m)u_p = 0, \quad (2)$$

where $\hat{p} = \gamma^0 E - \boldsymbol{\gamma} \mathbf{p}$. Multiplying by $(\hat{p} + m)$ and requiring that $u_p \neq 0$ one obtains the equation $E^2 - \mathbf{p}^2 - m^2 = 0$ which has two solutions

$$E^\pm(\mathbf{p}) = \pm \sqrt{\mathbf{p}^2 + m^2}. \quad (3)$$

Here the + sign corresponds to particles with positive energy $E_N(\mathbf{p}) = E^+(\mathbf{p})$, while the – sign corresponds to solutions with negative energy. To ensure stability of the physical vacuum Dirac has assumed that these negative-energy states are occupied forming what is called now the Dirac sea. Then the second solution of Eq. (3) receives natural interpretation: it describes holes in the Dirac sea.

These holes are identified with antiparticles. Their energies are obviously given by $E_{\bar{N}}(\mathbf{p}) = -E^{-}(-\mathbf{p}) = \sqrt{\mathbf{p}^2 + m^2}$. Unfortunately, the Dirac sea brings divergent contributions to physical quantities such as energy density, and one should introduce a proper regularization scheme to get rid of these divergences. This picture has received numerous confirmations in quantum electrodynamics and other fields.

Adiabatic dynamics of heavy nuclear system

One of the most fascinating aspects is the structure of the vacuum in QED and its change into charged vacuum states under the influence of strong (supercritical) electric fields.¹ We shortly remind of this phenomenon.

Figure 1 shows the diving of the deeply bound states into the lower energy continuum of the Dirac equation.

In the supercritical case the dived state is degenerate with the (occupied) negative electron states. Hence spontaneous e^+e^- pair creation becomes possible, where an electron from the Dirac sea occupies the additional state, leaving a hole in the sea which escapes as a positron while the electron's charge remains near the source. This is a fundamentally new process, whereby the neutral vacuum of QED becomes unstable in supercritical electrical fields. It decays within about 10^{-19} s into a charged vacuum. The charged vacuum is now stable due to the Pauli principle, that is the number of emitted particles remains finite. The vacuum is first charged twice because two electrons with opposite spins can occupy the $1s$ shell. After the $2p_{1/2}$ shell has dived beyond $Z_{cr} = 185$, the vacuum is charged four times, etc. This

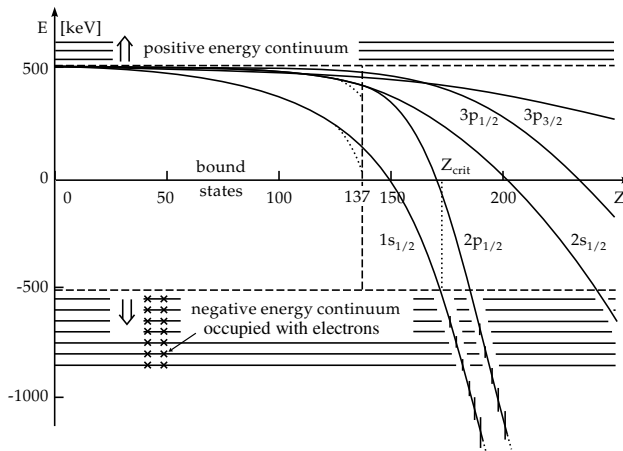


Fig. 1. Lowest bound states of the Dirac equation for nuclei with charge Z . While the Sommerfeld fine-structure energies (dashed line) for $\xi = 1$ (s states) end at $Z = 137$, the solutions for extended Coulomb potentials (full line) can be traced down to the negative-energy continuum reached at the critical charge Z_{cr} for the $1s$ state. The bound states entering the continuum obtain a spreading width as indicated.

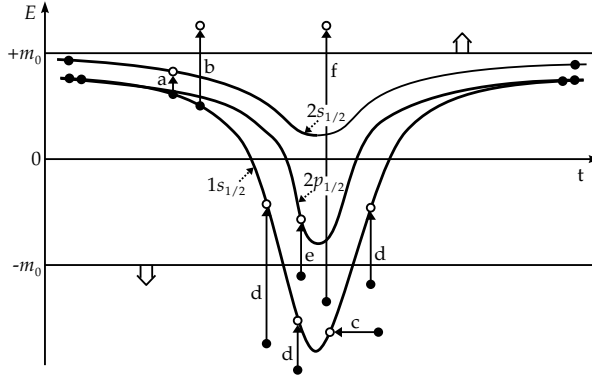


Fig. 2. Time dependence of the quasi-molecular energy levels in a supercritical heavy ion collision. The arrows denote various excitation processes which lead to the production of holes and positrons.

change of the vacuum structure is not a perturbative effect, as are the radiative QED effects (vacuum polarization, self-energy, etc.).

The time-dependence of the energy levels in a supercritical heavy ion collision is depicted in Fig. 2. An electron (or hole) which was in a certain molecular eigenstate at the beginning of the collision can be transferred with a certain probability into different states by the dynamics of the collision. This can lead to the hole production in an inner shell by excitation of an electron to a higher state and/or hole production by ionization of an electron to the continuum. Further possibilities are induced positron production by excitation of an electron from the lower continuum to an empty bound level and direct pair production.²

A comparison of the theoretical predictions and expectations and experimental data is shown in Fig. 3. Sharp positron peaks can be expected if there were a

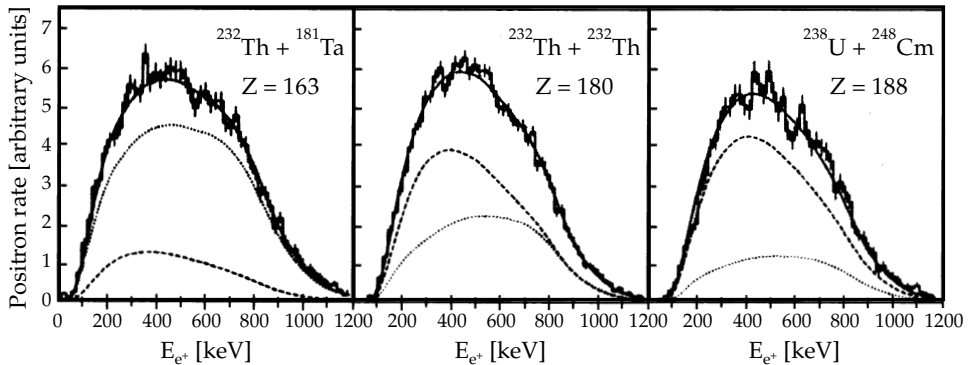


Fig. 3. Positron energy spectra measured in collisions of Th+Ta, Th+Th, and U+Cm at energies of about 6 MeV per nucleon. The QED predictions (dashed lines) and the experimentally determined background from nuclear pair conversion (dotted lines) add up to the full lines which are in close agreement with experiment.

mechanism in the heavy ion collision leading to a time delay. This may be caused by a pocket in the potential between the two ions. Spontaneous pair production should then be enhanced in supercritical systems. Until now, however, the situation remains inconclusive.²

2. Extreme Neutron-Rich Nuclei Ante Portas

I emphasize also the very interesting extension of the periodic table to extremely neutron rich isotopes of light nuclei. K. Gridnev and I have predicted such isotopes, e.g. ^{40}O , and others, for a number of years (Fig. 4). Some references are listed in Ref. 3. The recent experimental findings by the Michigan State group are supporting these ideas. This is fascinating!

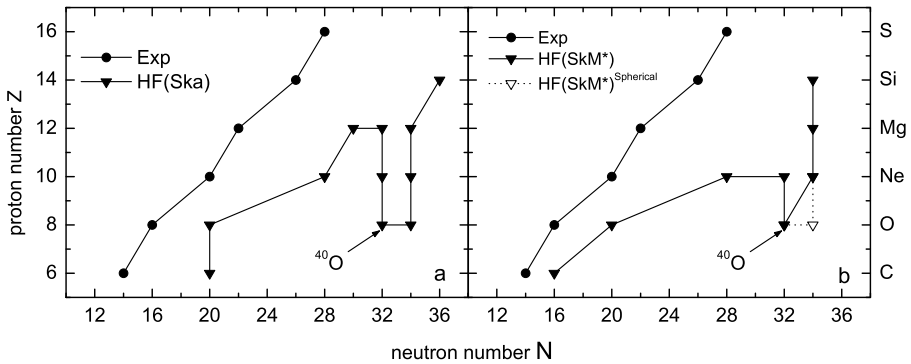


Fig. 4. Fragment of the neutron drip line given by our calculations [K.A. Gridnev et al., Eur. Phys. J. A direct (2005) DOI: 10.1140/epjad/i2005-06-027-y; Phys. of Part. and Nucl. Lett. V.2 No.6 359 (2005).] for Ska (fig. a) and SkM* (fig. b) forces. For each Z the plot shows the last heaviest experimentally known stable isotope [G. Audi et al., (2003)]. The unfilled triangle corresponds to the SHF calculations under the assumption of spherical symmetry.

3. On Superheavy Element Formation and Beyond

Superheavy (SH) nuclei obtained in “cold” fusion reactions with Pb or Bi target⁴ are along the proton drip line and very neutron-deficient with a short half-life. In fusion of actinides with ^{48}Ca more neutron-rich SH nuclei are produced⁵ with much longer half-life. But they are still far from the center of the predicted “island of stability” formed by the neutron shell around $N=184$ (see the nuclear map in Fig. 5). In the “cold” fusion, the cross sections of SH nuclei formation decrease very fast with increasing charge of the projectile and become less than 1 pb for $Z>112$. Heaviest transactinide, Cf, which can be used as a target in the second method, leads to the SH nucleus with $Z=118$ being fused with ^{48}Ca . Using the next nearest elements instead of ^{48}Ca (e.g., ^{50}Ti , ^{54}Cr , etc.) in fusion reactions with actinides is expected less encouraging, though experiments of such kind are planned to be

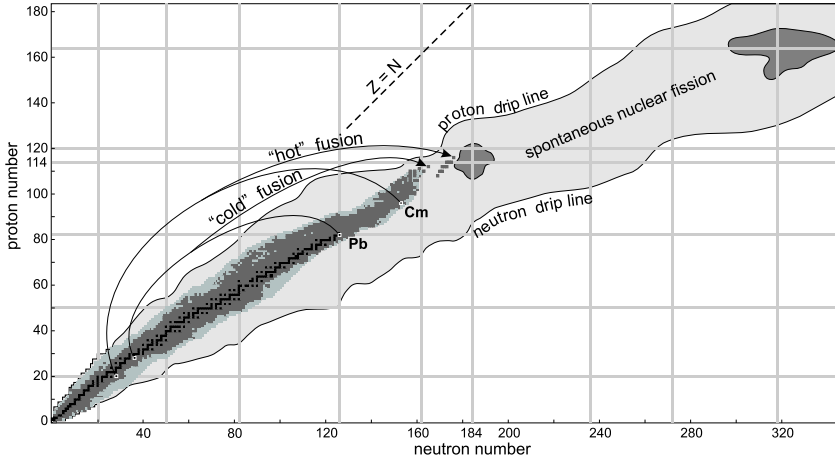


Fig. 5. Nuclear map. Predicted islands of stability are shown around $Z=114$, $N=184$ and $Z=164$, $N=318$.

performed. In this connection other ways to the production of SH elements in the region of the “island of stability” should be searched for.

About twenty years ago transfer reactions of heavy ions with ^{248}Cm target have been evaluated for their usefulness in producing unknown neutron-rich actinide nuclides.^{6,7} The cross sections were found to decrease very rapidly with increasing atomic number of surviving target-like fragments. However, Fm and Md neutron-rich isotopes have been produced at the level of $0.1 \mu\text{b}$. Theoretical estimations for production of primary superheavy fragments in the damped U+U collision have been also performed at this time within the semiphenomenological diffusion model.⁸ In spite of high probabilities obtained for the yields of superheavy primary fragments (more than 10^{-2} mb for $Z=120$), the cross sections for production of heavy nuclei with low excitation energies were estimated to be rather small: $\sigma_{CN}(Z = 114, E^* = 30 \text{ MeV}) \sim 10^{-6}$ mb for U+Cm collision at 7.5 MeV/nucleon beam energy. The authors concluded, however, that “fluctuations and shell effects not taken into account may considerably increase the formation probabilities.”

Here we study the processes of low energy collisions of very heavy nuclei (such as U+Cm) within the recently proposed model of fusion-fission dynamics.⁹ The purpose is to find an influence of the nearest closed shells $Z=82$ and $N=126$ (formation of ^{208}Pb as one of the primary fragments) on nucleon rearrangement between primary fragments. We try to estimate how large the charge and mass transfer can be in these reactions and what the cross sections for production of surviving neutron-rich SH nuclei are. Direct time analysis of the collision process allows us to estimate also the lifetime of the composite system consisting of two touching heavy nuclei with total charge $Z > 180$. Such “long-lived” configurations may lead to spontaneous positron emission from super-strong electric fields of quasi-atoms by a fundamental

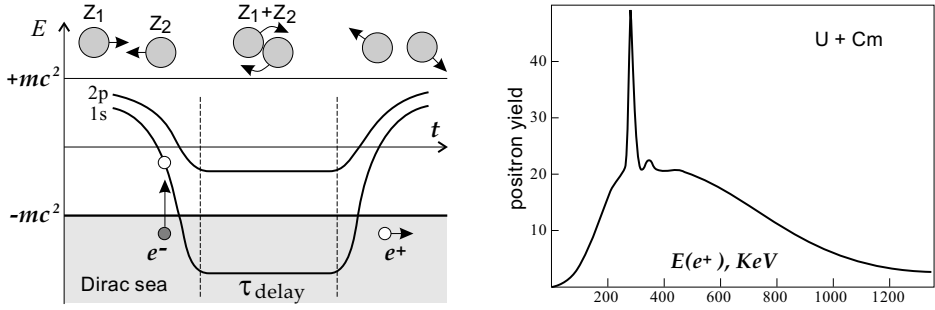


Fig. 6. Schematic figure of spontaneous decay of the vacuum and spectrum of the positrons formed in supercritical electric field ($Z_1 + Z_2 > 173$).

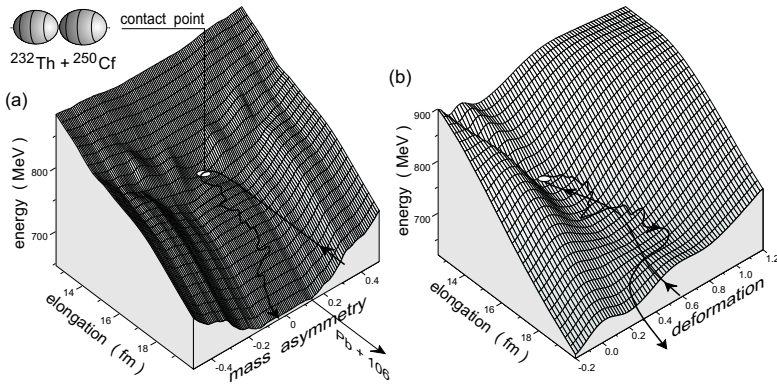


Fig. 7. Potential energy surface for the nuclear system formed by $^{232}\text{Th} + ^{250}\text{Cf}$ as a function of R and α ($\beta = 0.22$) (a), and R and β ($\alpha = 0.037$) (b). Typical trajectory is shown by the thick curves with arrows.

QED process (transition from neutral to charged QED vacuum),^{10,11} see schematic Fig. 6.

Besides the distance between the nuclear centers, R , the mass transfer, $\alpha = (A_1 - A_2)/(A_1 + A_2)$ and dynamic deformations of nuclear surfaces, β , play a most important role in fusion-fission and deep inelastic processes of low energy heavy ion collisions. The corresponding multi-dimensional adiabatic potential energy surface was calculated here within the semi-empirical two-core approach¹² based on the two-center shell model idea.¹³ Projections onto the $R - \alpha$ and $R - \beta$ planes of the three-dimensional potential energy are shown in Fig. 7 for the nuclear system formed in collision of $^{232}\text{Th} + ^{250}\text{Cf}$. There is no potential pocket typical for lighter systems, the potential is repulsive everywhere. However, the potential energy is not as steep in the region of contact point and two nuclei may keep in contact for a long time increasing their deformations and transferring nucleons to each other (see below).

We studied the whole dynamics of such a nuclear system by numerical solution of the coupled Langevin-type equations of motion, inertialess motion along the mass-asymmetry coordinate was derived just from the corresponding master equation for nucleon transfer.⁹ The inertia parameters μ_R and μ_β were calculated within the Werner–Wheeler approach.¹⁴ Parameters of the friction forces and nucleon transfer rate were taken from Ref. 9, where they have been estimated from successful description of experimental regularities of heavy ion deep inelastic scattering and fusion-fission reactions. Damping of the shell effects due to the excitation energy has been taken into account in the level density parameter both on the dynamic stage of the reaction and in statistical treatment of decay of the primary fragments.

The cross sections are calculated in a natural way. A large number of events (trajectories) are tested for a given impact parameter. Each event in studied reactions ends in the exit channel with two excited primary fragments. The corresponding double differential cross-section is calculated as follows

$$\frac{d^2\sigma_\alpha}{d\Omega dE}(E, \theta) = \int_0^\infty b db \frac{\Delta N_\alpha(b, E, \theta)}{N_{\text{tot}}(b)} \frac{1}{\sin(\theta)\Delta\theta\Delta E}. \quad (4)$$

Here $\Delta N_\alpha(b, E, \theta)$ is the number of events at a given impact parameter b in which the system enters into the channel α with kinetic energy in the region $(E, E + \Delta E)$ and center-of-mass outgoing angle in the region $(\theta, \theta + \Delta\theta)$, $N_{\text{tot}}(b)$ is the total number of simulated events for a given value of impact parameter.

The expression (4) describes the energy, angular, charge and mass distributions of the *primary* fragments formed in the reaction. Subsequent de-excitation of these fragments via fission or emission of light particles and gamma-rays was taken into account within the statistical model leading to the *final* fragment distributions. The sharing of the excitation energy between the primary fragments was assumed to be proportional to their masses. These fragments possess also some definite deformations at scission configuration. We assumed that the dynamic deformation relaxes rather fast to the ground state deformation (faster than neutron evaporation) and simply added the deformation energy to the total excitation energy of a given nucleus. Neutron emission during an evolution of the system was also taken into account. However, it was found that the pre-separation neutron evaporation does not influence significantly the final distributions.

Damped collisions of transuranium nuclei

Found in such a way mass and charge distributions of the primary and survived fragments formed in the $^{232}\text{Th}+^{250}\text{Cf}$ collision at 800 MeV center-of mass energy are shown in Fig. 8. The pronounced shoulder can be seen in the mass distribution of the primary fragments near the mass number $A=208$. It could be explained by existence of noticeable valley on the potential energy surface [see Fig. 7(a)], which corresponds to formation of doubly magic nucleus ^{208}Pb ($\alpha = 0.137$). The emerging

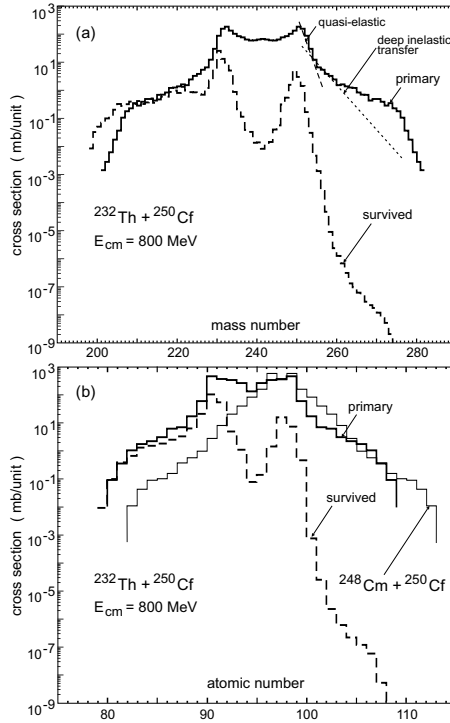


Fig. 8. Mass (a) and charge (b) distributions of primary (solid histograms) and survived (dashed histograms) fragments in the $^{232}\text{Th} + ^{250}\text{Cf}$ collision at 800 MeV center-of-mass energy. Thin solid histogram in (b) shows the primary fragment distribution in the hypothetical reaction $^{248}\text{Cm} + ^{250}\text{Cf}$.

of the nuclear system into this valley resembles the well-known quasi-fission process and may be called “inverse (or anti-symmetrizing) quasi-fission” (the final mass asymmetry is larger than initial one). For $\alpha > 0.137$ (one fragment becomes lighter than lead) the potential energy sharply increases and the mass distribution of the primary fragments falls down rapidly at $A < 208$ ($A > 274$). The same is for the charge distribution at $Z < 82$ ($Z > 106$). As a result, in the charge distribution of survived heavy fragments, Fig. 8(b), there is also a shoulder at $Z = 106$ and the yield of nuclei with $Z > 107$ was found in this reaction at the level of less than 1 pb. This result differs sharply from those obtained within the diffusion model,⁸ where the yield of heavy primary fragments decreases slowly and monotonically with increasing charge number.

In Fig. 9 the available experimental data on the yield of SH nuclei in collisions of $^{238}\text{U} + ^{238}\text{U}$ (Ref. 15) and $^{238}\text{U} + ^{248}\text{Cm}$ (Ref. 6) are compared with our calculations. In these experiments thick targets have been used, which means that the experimental data were, in fact, integrated over the energy in the region of about $750 \div 850$ MeV (Ref. 15, 6). The estimated excitation functions for the yield of heavy

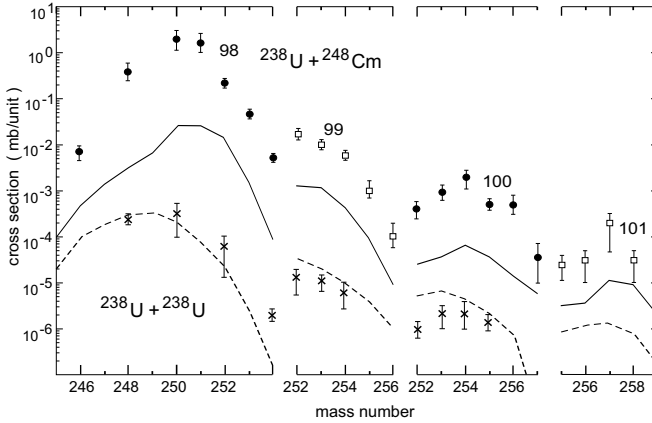


Fig. 9. Isotopic yield of the elements 98÷101 in the reactions $^{238}\text{U}+^{238}\text{U}$ (crosses)¹⁵ and $^{238}\text{U}+^{248}\text{Cm}$ (circles and squares).⁶ The curves show the result of our calculations.

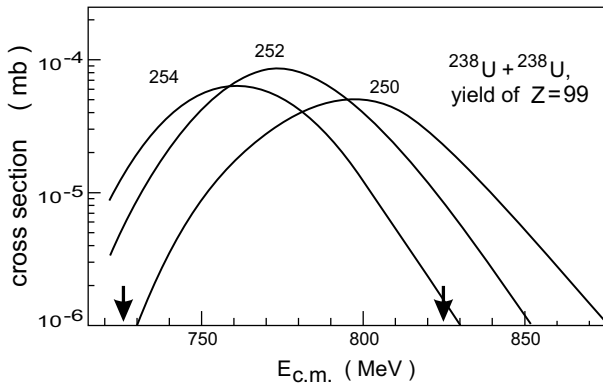


Fig. 10. Excitation functions for the yields of Es isotopes (numbers near the curves) for the $^{238}\text{U}+^{238}\text{U}$ reactions. The arrows indicate potential energy of two nuclei in contact ($r_0 = 1.16$ fm) for tip or nose-to-nose (left) and side or belly-to-belly (right) configurations.

surviving nuclei, shown in Fig. 10, demonstrate not so sharp as in fusion reactions but still rather strong dependence on beam energy. In spite of that, the agreement of our calculations with experimental data is quite acceptable (worse for few-nucleon transfer and better for massive transfer processes).

The estimated isotopic yields of SH nuclei in the $^{232}\text{Th}+^{250}\text{Cf}$, $^{238}\text{U}+^{238}\text{U}$ and $^{238}\text{U}+^{248}\text{Cm}$ collisions at 800 MeV center-of-mass energy are shown in Fig. 11. Thus there is a real chance for production and chemical study of the long-lived neutron-rich SH nuclei up to $^{274}_{107}\text{Bh}$ produced in the reaction $^{232}\text{Th}+^{250}\text{Cf}$. As can be seen from Figs. 10 and 11 the yield of SH elements in damped reactions depends strongly on beam energy and on nuclear combination which should be chosen care-

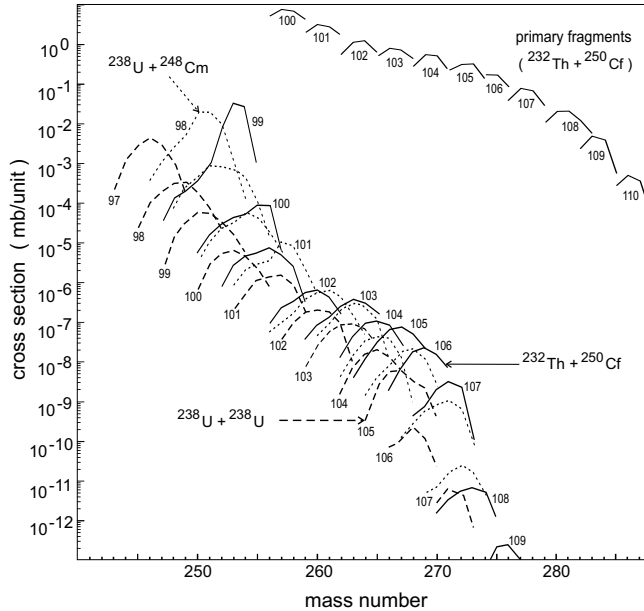


Fig. 11. Yield of superheavy nuclei in collisions of $^{238}\text{U}+^{238}\text{U}$ (dashed), $^{238}\text{U}+^{248}\text{Cm}$ (dotted) and $^{232}\text{Th}+^{250}\text{Cf}$ (solid lines) at 800 MeV center-of-mass energy. Solid curves in upper part show isotopic distribution of primary fragments in the Th+Cf reaction. In the case of U+Cm the upper curve only is marked by Z-number ($Z=98$), the others are one by one up to $Z=107$.

fully. In particular, in Fig. 8 the estimated yield of the primary fragments obtained in the hypothetical reaction $^{248}\text{Cm}+^{250}\text{Cf}$ (both constituents are radioactive) is shown, demonstrating a possibility for production of SH neutron-rich nuclei up to the element 112 (complementary to lead fragments in this reaction).

Giant quasi-atoms and spontaneous positron formation

The time analysis of the reactions studied shows that in spite of non-existing attractive potential pocket the system consisting of two very heavy nuclei may hold in contact rather long in some cases. During this time it moves over multidimensional potential energy surface with almost zero kinetic energy (result of large nuclear viscosity), a typical trajectory is shown in Fig. 7. The total reaction time distribution, $\frac{d\sigma}{d\log(\tau)}$ (τ denotes the time after the contact of two nuclei), is shown in Figs. 12 and 13 for the $^{238}\text{U}+^{248}\text{Cm}$ collision. We found that the dynamic deformations are mainly responsible here for the time delay of the nucleus-nucleus collision. Ignoring the dynamic deformations in the equations of motion significantly decreases the reaction time, whereas the nucleon transfer influences the time distribution not so strongly, see Fig. 12(a).

As mentioned above, the lifetime of a giant composite system more than 10^{-20} s is quite enough to expect for spontaneous e^+e^- production from the strong electric

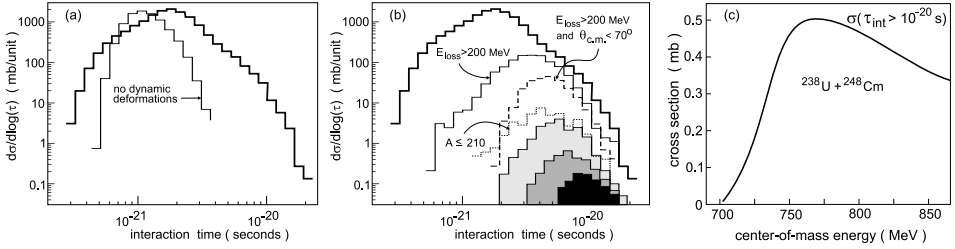


Fig. 12. Reaction time distributions for the $^{238}\text{U}+^{248}\text{Cm}$ collision at 800 MeV center-of-mass energy. Thick solid histograms correspond to all events with energy loss more than 30 MeV. (a) Thin solid histogram shows the effect of switching-off dynamic deformations. (b) Thin solid, dashed and dotted histograms show reaction time distributions in the channels with formation of primary fragments with $E_{\text{loss}} > 200$ MeV, $E_{\text{loss}} > 200$ MeV and $\theta_{\text{c.m.}} < 70^\circ$ and $A \leq 210$, correspondingly. Hatched areas show time distributions of events with formation of the primary fragments with $A \leq 220$ (light gray), $A \leq 210$ (gray), $A \leq 204$ (dark) having $E_{\text{loss}} > 200$ MeV and $\theta_{\text{c.m.}} < 70^\circ$. (c) Cross section for events with interaction time longer than 10^{-20} s depending on beam energy.

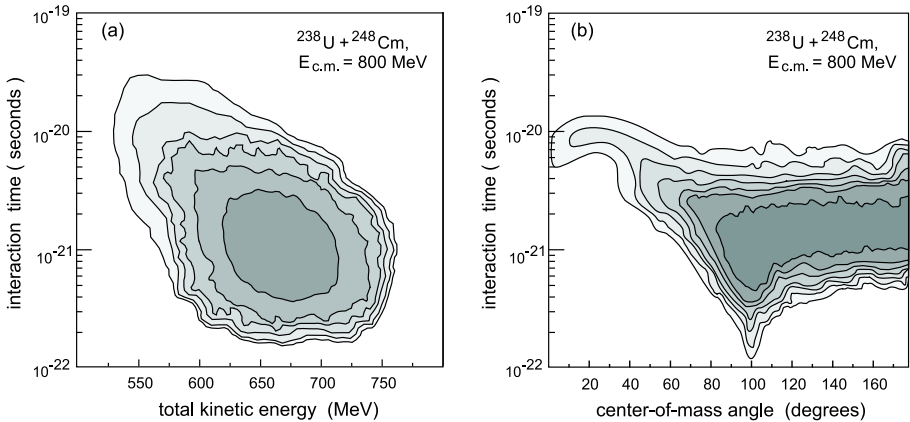


Fig. 13. Energy-time (a) and angular-time (b) distributions of primary fragments in the $^{238}\text{U} + ^{248}\text{Cm}$ collision at 800 MeV ($E_{\text{loss}} > 15$ MeV). The landscape is shown in logarithmic scale — lines are drawn over one order of magnitude. The quasi-elastic peak is removed.

field as a fundamental QED process (“decay of the vacuum”).^{10,11} The absolute cross section for long events ($\tau > 10^{-20}$ s) was found to be maximal just at the beam energy ensuring two nuclei to be in contact, see Fig. 12(c). Note that the same energy is also optimal for production of the most neutron-rich SH nuclei (Fig. 10). Of course, there are some uncertainties in the used parameters, mostly in the value of nuclear viscosity. However we found only a linear dependence of the reaction time on the strength of nuclear viscosity, which means that the obtained reaction time distribution is rather reliable, see logarithmic scale on both axes in Fig. 12(a).

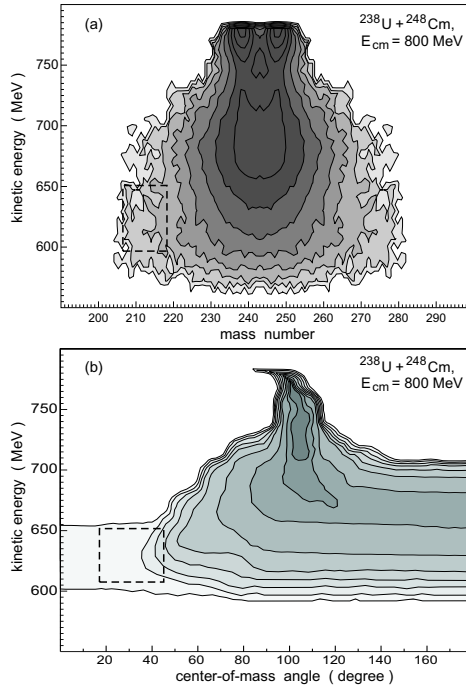


Fig. 14. Energy-mass (a) and energy-angular (b) distributions of primary fragments in the $^{238}\text{U} + ^{248}\text{Cm}$ collision at 800 MeV ($E_{\text{loss}} > 15$ MeV). Logarithmic landscape of the corresponding double differential cross sections. Lines are drawn over each half order of magnitude. The dashed rectangles show the regions of the longest events.

Formation of the background positrons in these reactions forces one to find some additional trigger for the longest events. Such long events correspond to the most damped collisions with formation of mostly excited primary fragments decaying by fission. However there is also a chance for production of the primary fragments in the region of doubly magic nucleus ^{208}Pb , which could survive against fission due to nucleon evaporation, see Figs. 14(a) and 8. The number of the longest events depends weakly on impact parameter up to some critical value. On the other hand, in the angular distribution of all the excited primary fragments (strongly peaked at the center-of-mass angle slightly larger than 90°) there is the rapidly decreasing tail at small angles, see Fig. 14(b). Thus the detection of the surviving nuclei in the lead region at the center-of-mass angles less than 60° could be a definite witness for a long reaction time.

The production of long-lived neutron-rich SH nuclei in collisions of transuranium ions seems to be quite possible due to a large mass and charge rearrangement in the “inverse quasi-fission” process caused by the $Z=82$ and $N=126$ nuclear shells. Radiochemical identification of $^{267,268}\text{Db}$ isotopes, produced in the $\text{U} + \text{Cm}$ or $\text{Th} + \text{Cf}$ reactions, could be performed, for example, to test this conclusion. If the found cross section will be higher than 10 pb, then the subsequent experiments with such

reactions could be planned aimed to the production of SH nuclei just in the region of the “island of stability”. Parallel search for spontaneous positron emission from a supercritical electric field of long-lived quasi-atoms formed in these reactions is also quite promising.

4. Concluding Remarks — Outlook

The extension of the periodic system into the sectors hypermatter (strangeness) and antimatter is of general and astrophysical importance. Indeed, microseconds after the big bang the new dimensions of the periodic system, we have touched upon, certainly have been populated in the course of the baryo- and nucleogenesis. Of course, for the creation of the universe, even higher dimensional extensions (charm, bottom, top) come into play, which we did not pursue here. It is an open question, how the depopulation (the decay) of these sectors influences the distribution of elements of our world today. Our conception of the world will certainly gain a lot through the clarification of these questions.

The experimental verification of the decay of the vacuum is most important. A fundamental process like this must be experimentally clarified and soundly based. I hope that the proposed triggers for long time delay in the formation of giant nuclear systems may help to bring this important fundamental physics forward.

One of our goals has also been to demonstrate that energetic antiproton beams can be used to study new interesting phenomena in nuclear physics. We discuss the possible existence of a completely new kind of strongly interacting systems where both the nucleons and the antinucleons coexist within the same volume and where annihilation is suppressed due to the reduction of the available phase space. Such systems are characterized by large binding energy and high nucleon density. Certainly, antinucleons can be replaced by antihyperons or even by antiquarks. We have presented the first self-consistent calculation of a finite nuclear system containing one antiproton in a deeply bound state. For this study we have used several versions of the RMF model which give excellent description of ordinary nuclei. The presence of an antiproton in a light nucleus like ^8Be or ^{16}O changes drastically the whole structure of the nucleus leading to a much more dense and bound state. In heavy systems the presence of a few antinucleons distorts and deforms the nuclear system leading to a localized central region of highly increased density. This is a mechanism for cold compression. We also found that nuclear systems with total baryon number zero show extremely deep and symmetric states.

It is clear however that these structural changes can occur only if the life time of the antibaryons in the nuclear interior is long enough.

One should bear in mind that originally the RMF model was formulated within the Hartree and no-sea approximations. Implementing the Dirac sea may require serious revision of the model and inclusion of additional terms. Hartree calculations including the Dirac sea and Hartree-Fock calculations including exchange terms lead to smaller nucleon potentials in normal nuclei. Shallower potentials will produce

smaller attraction for antinucleons, but the qualitative effect that the presence of antiprotons reduces repulsion and enhances attraction for nucleons will remain valid. We expect that the additional binding and compression of the nucleus will appear even for an antinucleon potential as low as 200 MeV.

In summary, on the basis of the RMF model we have studied the structure of nuclear systems containing a few real antibaryons. We have demonstrated that the antibaryons act as strong attractors for the nucleons leading to enhanced binding and compression of the recipient nucleus. As our estimates show the life times of antibaryons in the nuclear environment could be significantly enhanced due to the reduction of the phase space available for annihilation. Narrow peaks in the pion or kaon spectra at the energy around 1 GeV are proposed as the most clear signature of deeply-bound antibaryon states in nuclei.

For the Gesellschaft für Schwerionenforschung (GSI), which I helped initiating in the sixties, the questions raised here could point to the way ahead. The FAIR project, meanwhile approved by the funding agencies, can — at least to some extent — follow this path.

Indeed, what is needed is a **vision on a long term basis**. The ideas proposed here, the verification of which will need the **commitment for 2–4 decades of research**, could be such a vision with considerable attraction for the best young physicists. The new dimensions of the periodic system made of hyper- and antimatter cannot be examined in the “stand-by” mode at CERN (Geneva); a dedicated facility is necessary also for this field of research, which can in future serve as a home for the universities. The GSI — which has unfortunately become much too self-sufficient — could be such a home for new generations of physicists, who are interested in the **structure of elementary matter**. GSI would then not develop just into a detector laboratory for CERN, and as such become obsolete. I can already see the enthusiasm in the eyes of young scientists, when I unfold these ideas to them — similarly as it was more than 35 years ago, when the nuclear physicists in the state of Hessen initiated the construction of GSI.

References

1. W. Greiner, B. Müller, J. Rafelksi, *Quantum electrodynamics of strong fields*, Springer Verlag, 2nd edition, December 1985.
2. J. Reinhardt and W. Greiner, *Quantum electrodynamics*, Springer Verlag, 3rd edition, February 2003.
3. a. K.A. Gridnev, D.K. Gridnev, V.G. Kartavenko, V.E. Mitroshin, V.N. Tarasov, D.V. Tarasov, W. Greiner,
About a stability of nuclei with neutron excess, ENAM'04, IV Int. Conf. on Exotic Nuclei and Atomic Masses, September 12-16, 2004 Callaway Gardens, Pine Mountain, Georgia, USA. Abstracts (2004) p.335.
b. K.A. Gridnev, D.K. Gridnev, V.G. Kartavenko, V.E. Mitroshin, V.N. Tarasov, D.V. Tarasov, W. Greiner
Stability island near the neutron-rich ^{40}O isotope, The Eur. Phys. Journal A direct (2005) DOI: 10.1140/epjad/i2005-06-027-y.

- c. K.A. Gridnev, D.K. Gridnev, V.G. Kartavenko, V.E. Mitroshin, V.N. Tarasov, D.V. Tarasov, W. Greiner
Neutron-rich nuclei near the drip-line for $6 \leq Z \leq 16$, LV National Conf. on Nucl. Phys. "Frontiers in the Physics of Nucleus" June 28-July 1, 2005, St. Petersburg, Russia. Book of Abstracts. p.134.
- d. K.A. Gridnev, D.K. Gridnev, V.G. Kartavenko, V.E. Mitroshin, V.N. Tarasov, D.V. Tarasov, W. Greiner,
On Stability of Neutron-Rich Nuclei, Physics of Particles and Nuclei Letters, Vol. 2, No. 6, 2005, pp. 359-363.
- e. K.A. Gridnev, D.K. Gridnev, V.G. Kartavenko, V.E. Mitroshin, V.N. Tarasov, D.V. Tarasov, W. Greiner,
Specific Features of the Nuclear Drip Line of Light Nuclei, Physics of Atomic Nuclei, 2006, Vol. 69, No. 1, pp. 1-5.
- f. K.A. Gridnev, D.K. Gridnev, V.G. Kartavenko, V.E. Mitroshin, V.N. Tarasov, D.V. Tarasov, W. Greiner,
On stability of the neutron-rich oxygen isotopes, Int. Jour. Mod. Phys. E 2006, V. 15, N.3, 673-683.
4. S. Hofmann and G. Münzenberg, Rev. Mod. Phys. **72**, 733 (2000).
 5. Yu.Ts. Oganessian, V.K. Utyonkov, Yu.V. Lobanov, F.Sh. Abdullin, A.N. Polyakov, I.V. Shirokovsky, Yu.S. Tsyganov, G.G. Gulbekian, S.L. Bogomolov, B.N. Gikal, A.N. Mezentsev, S. Iliev, V.G. Subbotin, A.M. Sukhov, A.A. Voinov, G.V. Buklanov, K. Subotic, V.I. Zagrebaev, M.G. Itkis, J.B. Patin, K.J. Moody, J.F. Wild, M.A. Stoyer, N.J. Stoyer, D.A. Shaughnessy, J.M. Kenneally, P.A. Wilk, R.W. Loughheed, R.I. Il'kaev, and S.P. Vesnovskii, Phys. Rev. C **70**, 064609 (2004).
 6. M. Schädel, W. Bröchle, H. Gäggeler, J.V. Kratz, K. Sümmerer, G. Wirth, G. Herrmann, R. Stakemann, G. Tittel, N. Trautmann, J.M. Nitschke, E.K. Hulet, R.W. Loughheed, R.L. Hahn, and R.L. Ferguson, Phys. Rev. Lett. **48**, 852 (1982).
 7. K.J. Moody, D. Lee, R.B. Welch, K.E. Gregorich, G.T. Seaborg, R.W. Loughheed, and E.K. Hulet, Phys. Rev. C **33**, 1315 (1986).
 8. C. Riedel, W. Nörenberg, Z. Phys. A **290**, 385 (1979).
 9. V. Zagrebaev and W. Greiner, J. Phys. G **31**, 825 (2005).
 10. J. Reinhard, U. Müller and W. Greiner, Z. Phys. A **303**, 173 (1981).
 11. W. Greiner (Editor), *Quantum Electrodynamics of Strong Fields*, (Plenum Press, New York and London, 1983); W. Greiner, B. Müller and J. Rafelski, *QED of Strong Fields* (Springer, Berlin and New York, 2nd edition, 1985).
 12. V.I. Zagrebaev, Phys. Rev. C **64**, 034606 (2001); in *Tours Symposium on Nucl. Phys. V*, AIP Conf. Proc., 2004, **704**, p. 31., see also invited talk at the IX International Conference on Nucleus Nucleus Collisions, Rio de Janeiro, Brazil, August 28 - September 1, 2006.
 13. U. Mosel, J. Maruhn, and W. Greiner, Phys. Lett. B **34**, 587 (1971); J. Maruhn and W. Greiner, Z. Phys. **251**, 431 (1972).
 14. F.G. Werner and J.A. Wheeler, unpublished; K.T.R. Davies, A.J. Sierk, and J.R. Nix, Phys. Rev. C **13**, 2385 (1976).
 15. M. Schädel, J.V. Kratz, H. Ahrens, W. Bröchle, G. Franz, H. Gäggeler, I. Warnecke, G. Wirth, G. Herrmann, N. Trautmann, and M. Weis, Phys. Rev. Lett. **41**, 469 (1978).